Highly Conducting, Strong Nanocomposites Based on Nanocellulose-Assisted Aqueous Dispersions of Single-Wall Carbon Nanotubes

Mahiar M. Hamedi,[†,⊥,*] Alireza Hajian,[‡,⊥] Andreas B. Fall,[‡,†] Karl Håkansson,[§] Michaela Salajkova,[‡] Fredrik Lundell,[§] Lars Wågberg,[‡,†] and Lars A. Berglund[‡]

[†]Department of Fibre and Polymer Technology, [‡]Wallenberg Wood Science Centre, [§]Department of Mechanics, KTH Royal Institute of Technology, Teknikringen 56, 100 44 Stockholm, Sweden. [⊥]These authors contributed equally.

ABSTRACT It is challenging to obtain high-quality dispersions of single-wall nanotubes (SWNTs) in composite matrix materials, in order to reach the full potential of mechanical and electronic properties. The most widely used matrix materials are polymers, and the route to achieving high quality dispersions of SWNT is mainly chemical functionalization of the SWNT. This leads to increased cost, a loss of strength and lower conductivity. In addition full potential of colloidal self-assembly cannot be fully exploited in a polymer matrix. This may limit the possibilities for assembly of highly ordered structural nanocomposites. Here we show that nanofibrillated cellulose (NFC) can act as an excellent aqueous dispersion agent for as-prepared SWNTs, making possible low-cost exfoliation and purification of SWNTs with dispersion limits exceeding 40 wt %. The NFC:SWNT dispersion may also offer a cheap and sustainable alternative for molecular self-assembly of advanced composites. We demonstrate semitransparent conductive films, aerogels and anisotropic microscale fibers with nanoscale composite structure. The NFC:SWNT nanopaper shows increased strength at 3 wt % SWNT, reaching a modulus of 13.3 GPa, and a strength of 307 MPa. The anisotropic microfiber composites have maximum conductivities above 200 S cm^{-1} and current densities reaching 1400 A cm^{-2}.

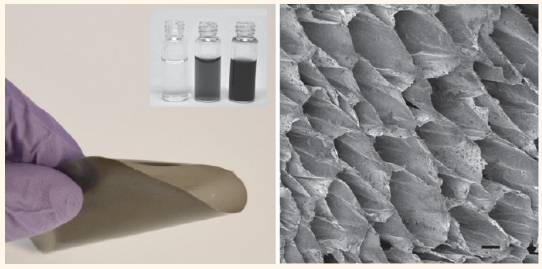

KEYWORDS: nanocellulose · nanopaper · carbon nanotubes · dispersions · composites · conductivity · self-assembly

Carbon nanotubes (CNTs) are one of the most important nanomaterial components. They have been exploited in numerous fields including composites, energy storage, biotechnology, formation of coatings and films, and microelectronics.[1] Individual CNTs are among the strongest[2,3] and most conductive nanomaterials known, and therefore of great interest for nanocomposites. Single-wall nanotubes (SWNTs) can both add conductivity, and increase the mechanical strength of the composite.[4] Synthetic polymers is the most exploited matrix material class for nanotubes. The fabrication of CNT/polymer composites requires dispersion of the nanotubes in a polymer matrix. In general, dispersion is necessary to separate CNT bundles into stable few or single CNT colloid particles.[5] This facilitates cleaning from impurities, separation, and self-assembly into the desired structures. For composites in particular, high quality dispersion of the nanoenforcement in the matrix is necessary to achieve the best possible mechanical, and electronic properties, at reasonable volume fractions.[6] Chemical functionalization of CNTs has been used extensively in order to improve dispersion.[7] However, chemical functionalization substantially increases the CNT price and disrupts the electronic network of the nanotubes. In addition, the presence of polymer and grafted functional groups limit the nanotube to nanotube carrier hopping so that conductivities are decreased.[8]

As an alternative to synthetic polymers, composites based on low-cost nanomaterials

* Address correspondence to mahiar@kth.se.

Received for review November 22, 2013 and accepted February 8, 2014.

Published online February 08, 2014
10.1021/nn4060368

from renewable resources are explored. One of the most promising materials is nanofibrillated cellulose (NFC), which is extracted from abundant native cellulose fibers and is a mesoscopic material with a length in the micrometer domain, and diameters of only a few nanometers.[9,10] These fibrils have excellent properties including high elastic modulus[11] (around 100 GPa crystal modulus) and low thermal expansion[12] (*ca.* 3 ppm K^{-1} in the axial direction). Both these properties are much superior to isotropic polymers making NFC an ideal material component for environmentally friendly high-strength composites[13] with excellent mechanical properties. It is desirable to add nanocomponents to the NFC dispersion for making functional hybrid composites. However, due to the very high colloidal stability and inherent strength of NFC, the addition of almost any material to NFC degrades the overall mechanical properties of the final hybrid composite. A promising candidate here is single-wall nanotubes SWNTs, which have a Young's modulus about an order of magnitude higher than NFC, on the single fiber scale. A few attempts have been made to mix CNTs[14−16] with NFCs. In these studies, the CNTs were first cleaned and dispersed in water using surfactants or covalent functionalization, and then mixed with the NFC dispersion. The surfactants greatly reduced the mechanical and electrical properties of these hybrid composites. For these reasons, it has not yet been possible to provide a route for the cheap production of highly conductive and stronger NFC composites. Indeed, all demonstrated NFC:SWNT composites have so far exhibited a decrease in mechanical properties with increasing CNT content, and the price of the starting CNT dispersions has been unreasonably high compared to that of the NFC.

Here we show a route for making cheap, strong, and highly conductive NFC composites. This is made possible by exploiting the novel discovery that NFC itself is an excellent dispersion and purification agent for SWNTs in water. Here we carefully analyze the dispersion properties of the NFC:SWNT and demonstrate a number of advanced NFC-based nanocomposites with better mechanical and electronic properties than any previously reported.

RESULTS AND DISCUSSION

In this study, we have focused on using carboxymethylated NFC with approximate diameters of 2−5 nm and lengths of 0.5−1 μm. (more details in Experimental Section and ref 17). We have further used untreated SWNTs, produced by high-pressure carbon monoxide disproportionation (HiPco). These SWNTs have bundle diameters in the range of 4−5 nm and lengths of 1−5 μm according to the manufacturer (Carbon Solutions, Inc.). The SWNTs were mixed from powder with NFC that was suspended in a dilute state (*ca.* 1 g/L). The mixture was subjected to ultrasonication and finally we used high speed centrifugation at 20 000*g* for purification and separation of SWNTs, based on previous reports[18] (see Experimental Section for details).

We assessed the quality of the dispersion of NFC:SWNT by performing UV−vis-NIR spectroscopy, Raman spectroscopy, dynamic light scattering and zeta potential measurements.

Figure 1a displays the UV−vis-NIR absorption spectra of NFC:SWNT dispersion (31 wt % SWNT, 1 g/L), where the characteristic band centered around 9800 cm^{-1} corresponds to the S_{22} interband transition in the semiconducting SWNTs, and the M_{11} peak at 13 800 cm^{-1} corresponds to the interband transition in metallic nanotubes. The widths of these peaks represent the inherent distribution of the diameters and chirality of the nanotubes based on the production method.

Figure 1b displays the Raman spectra of the NFC:SWNT dispersion (1 g/L NFC, 31 wt % SWNT). Here the G band is seen near 1590 cm^{-1}, which corresponds to the vibrational modes of the SWNTs, whereas the D band at around 1340 cm^{-1} is the Raman active mode with a value that is roughly proportional to the amount of amorphous carbon in the dispersion. The ratio of the maximum intensity value between the G and the D peak (G/D), therefore, quantifies the quality of the dispersion and was here calculated to be 25, thus showing successful purification.[19]

The radial breathing mode (RBM) in the Raman spectra is a rare feature of SWNTs with frequencies that are inversely proportional to the nanotube diameter. In Figure 1b, a narrow peak with a maximum at 185 cm^{-1}, therefore, indicates that we have a fairly narrow distribution of SWNT diameters, due to the present purification procedure. The width and shape of the peak is similar to previous results shown for SWNTs that have been both precleaned and dispersed with biopolymers such as carboxymethylcellulose.[20]

To study the colloidal stability, and the relative size distribution of the colloid particles, we performed dynamic light scattering (DLS) and zeta potential measurements. For the pure NFC dispersions at 0.1 g/L and neutral pH, a zeta potential of 60 ± 5 mV was recorded. More importantly, for the NFC:SWNT dispersion at a high SWNT content (30 wt % SWNT), a similar zeta potential was obtained. The unchanged value of the zeta potential indicated that the dispersion is indeed very stable, and also that the SWNTs have been dispersed without altering the repulsive electrostatic interactions between the NFC particles. Figure 1c shows the normalized intensity autocorrelation function for NFC and NFC:SWNT dispersions. The high intercept of the curves at $t_d = 0$, all above 0.8, indicates an ergodic system, *i.e.*, freely moving particles. Also, the sharp and consistent drop of the curves indicates that both pure NFC and the mixed NFC:SWNT system have a monomodal distribution in the size of the diffusing

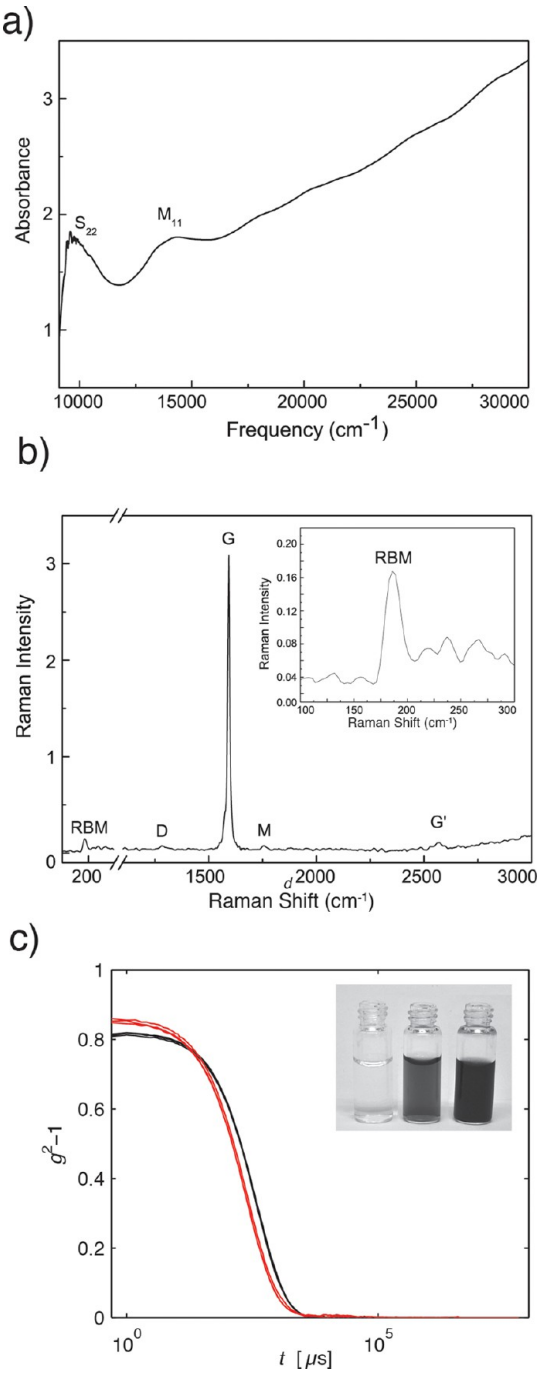

Figure 1. (a) UV−vis-NIR absorbance for SWNT dispersed in NFC in water (31 wt % SWNT, 1 g/L). (b) Raman spectra of SWNT dispersed and cleaned in NFC (1 g/L NFC, 31 wt % SWNT). (c) Dynamic light scattering data, showing the normalized intensity autocorrelation function ($g^2 - 1$) *vs* time (t_d) for pure NFC (blue) and a dispersion of 10 wt % SWNT in 0.1 g/L NFC (black). (Inset) Photographs showing (left) NFC in water, (middle, right) dispersions NFC:SWNT with different wt % of SWNT.

objects. Thus, the degree of aggregation/cluster formation is expected to be low. However, the correlation decreases at larger t_d in the mixed system compared to that of the pure system. This relaxation time increased by a factor of 1.5, indicating slower movement, and thus larger objects. This is natural, considering that the dispersion of NFC:SWNT consists of combinations of the two nanoparticles. The size is roughly increased by the same factor. This demonstrates that only slightly larger objects are present in the mixed system than in the pure NFC, and indicates that the SWNTs have indeed been successfully exfoliated into individual or small bundles of nanotubes and stabilized at these smaller sizes by association with the NFC nanoparticles.

To study the morphology of the NFC:SWNT dispersion, we used transmission electron microscopy (TEM) and atomic force microscopy (AFM) imaging (see Experimental Section details). Figure 2a shows the TEM image of a NFC:SWNT hybrid. It is difficult to clearly distinguish the SWNT from NFC from the width of the fibers; however, the longer, straight fibers with a predominantly vertical orientation most probably contain SWNTs (see black arrow). The kinked fibers with short distances between kinks should correspond to pure NFC fibers (see white arrow). It is known that amorphous regions between crystalline regions in NFC are mechanically weaker and can result in the kinks observed.[21] We also see similar kinked NFC fibers in pure NFC samples dried on a substrate (see AFM image in Figure 5S). At higher magnification in the TEM image, we also observed individual SWNT fibers and small bundles of SWNT (Figure 2S).

To further assess the dimensions, we used AFM imaging. Figure 2b displays height values for the NFC:SWNT fibers dried from the dispersion. The nanofibers are mostly in the range of a few to less than 10 nm, which corresponds well with individual or small bundles of either NFC or SWNTs. The nanoscopy results, therefore, provide support that we have indeed achieved successful dispersion and purification of the SWNTs. The results also indicate that the dispersion is stable during drying, which is important for preparation of nanocomposites.

Together, the experimental results show that NFC can successfully disperse SWNTs into individual or small SWNT bundles of stable colloidal particles. It has previously been shown that polysaccharides[20,22] and nanowhiskers[23] can serve as dispersing agents for SWNTs in water, although the mechanism for the NFC dispersion property is not yet clear. The energy needed for dispersing SWNTs in water is large, due to its nonpolar character and large specific surface area, and this will promote aggregation of the SWNTs in water. It is also known that cellulose is strongly hydrated when dispersed in water. When the SWNT particles interact with the NFC dispersion, there will be significant van der Waals interaction, since cellulose has a fairly high nonpolar contribution to its surface energy.[24] Furthermore, if the SWNTs are adsorbed to the NFC, all the water associated with the NFC will be released resulting in a large increase in entropy. Considering the large specific surface area of the NFC, this effect will also be much greater compared with for

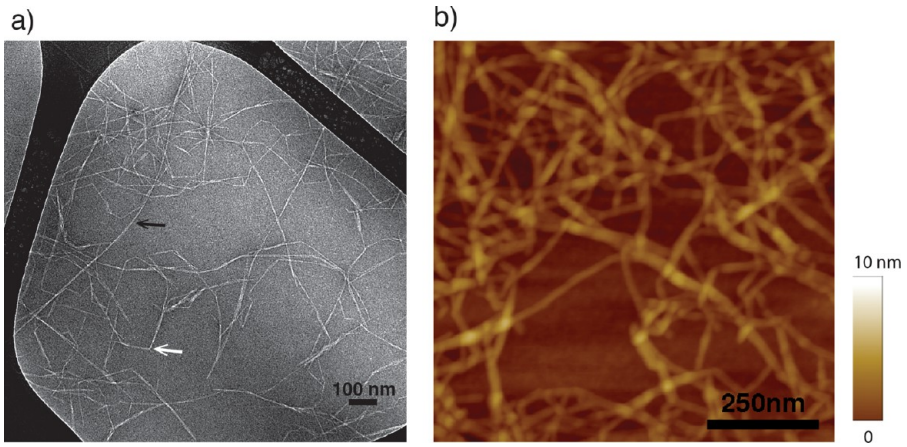

Figure 2. (a) TEM image of SWNT:NFC dried and uranyl acetate stained on a carbon-coated copper grid. Scalebar 100 nm. (b) Atomic force microscopy height images of NFC:SWNT dispersion dried on a silicon wafer. Scalebar 250 nm, and colorbar corresponding to height values.

example microscale cellulose pulp fibers. This could mean that the driving force for the dispersion of SWNTs by NFC should be an overall gain in entropy combined with the high nonpolar interaction between the two types of nanoparticles. From the collected images it is, however, not clear how nanoparticles are interacting. More work is needed to clarify the mechanisms by which the SWNTs are dispersed by the NFC.

The demonstrated procedure makes the large-scale and inexpensive production of high quality SWNT dispersions possible, and at the same time results in a nanoparticle blend that is suitable for aqueous self-assembly of functional nanocomposites. To demonstrate this, we designed and prepared different forms of nanocomposites. Generally, NFC composites can be made by first transforming the NFC dispersion from the dilute to a gel state, followed by drying of the gel to form the final composite. This offers numerous possibilities for creating a number of different nanostructures depending on the state of the fluid in the dilute system prior to gelation, the method of gelation, and the method of drying.

Dispersions with different ratios of SWNT to NFC were used to make nanopaper structures by vacuum filtration using a microfilter followed by drying in a sheet former (see Experimental Section details, schematics in Figure 3a, and photos of the nanopapers in Figure 3b). Different nanopapers were made by varying the initial SWNT to NFC weight ratio prior to dispersion. Since an unknown fraction of the SWNT is removed during the centrifugation purification process, the final SWNT concentration was measured by using UV−vis absorption and applying the Beer−Lambert's Law (for details see Experimental Section and Figure 3d).

The composite nanopaper was imaged using AFM in the phase imaging mode (Figure 3c). (We used phase imaging since the large roughness of the nanopaper did not allow clear height imaging.) The phase image showed that both the SWNT and NFC nanofibers in the nanopaper had random-in-the-plane orientation. Most of the nanotubes were below 10 nm in width, and this indicates that the dispersion was fairly stable during the nanopaper formation process.

The mechanical properties of the nanopaper structures were determined and compared with that of pure NFC nanopaper and pure SWNT "buckypaper", made from carboxylic acid functionalized SWNTs (SWNT-COOH) dispersed in water. The reason for choosing SWNT-COOH was that these could be dispersed using the same procedure as that used for the NFC:SWNT dispersion. Furthermore, the SWNT-COOH has the same ionic side group (carboxyl) as that of the NFC that is used here. The SWNT-COOH dispersion should therefore represent the closest approximation to the NFC:SWNT dispersion but without the NFC component.

Table 1 presents a summary of the mechanical properties of the different nanopapers. It should be noted here that pure nanopaper has a tensile strength around 300% higher, and a strain at failure around 1800% higher than the SWNT-COOH buckypaper. The addition of carbon nanotubes to the NFC composite is not therefore immediately expected to increase the mechanical properties. It is rather the addition of electronic properties with retained mechanical property function and the potential for controlled self-assembly which is the main objective.

In Table 1, the 3 wt % SWNT nanopaper, however, shows a slight increase of 6.4% in modulus and 2.6% in strength, compared to the pure NFC reference nanopaper. This indicates that the mechanical properties of the bicomponent dispersion should not be viewed as simply a superposition of the properties of its single components. The addition of more SWNT to the random network nanopaper composite led to a decreased modulus, strength and strain-to-failure. This could be a result of insufficient nanofiber−nanofiber interaction for favorable stress-transfer.

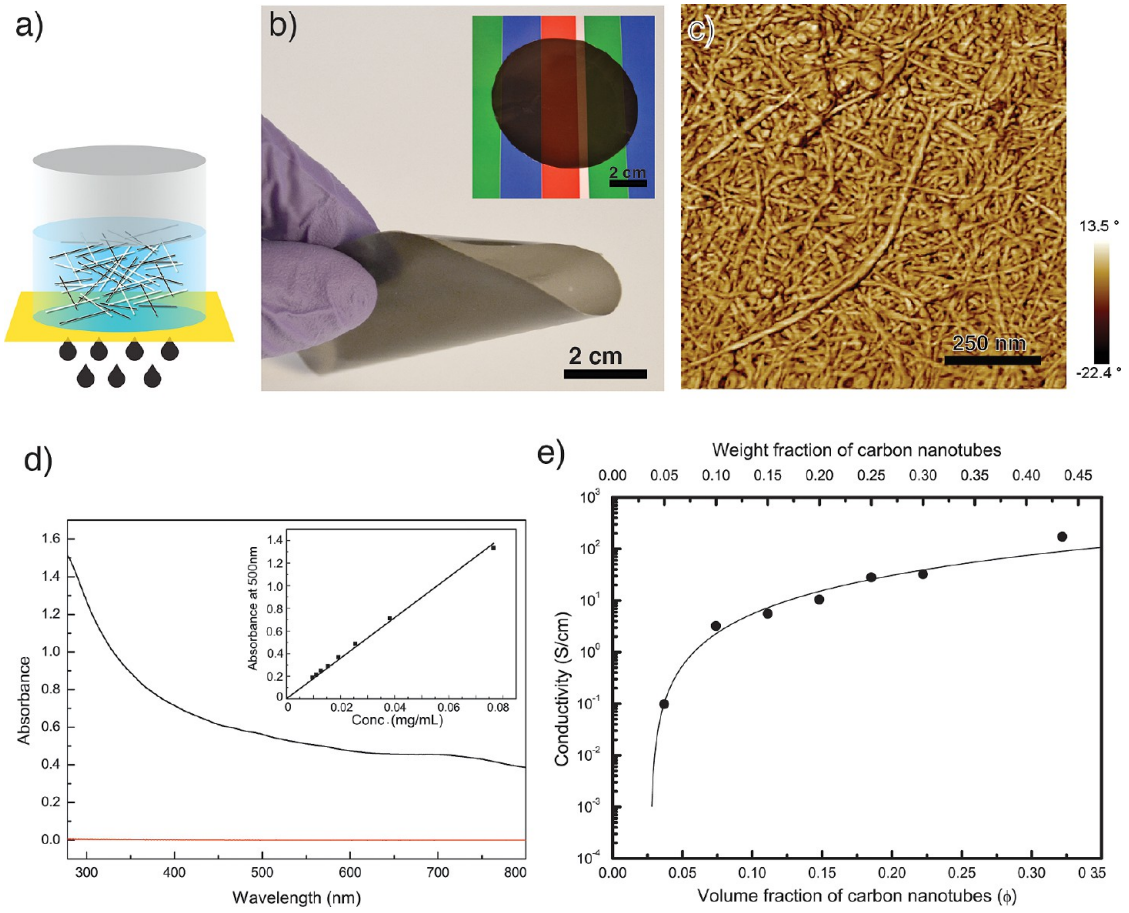

Figure 3. (a) Schematics of the preparation of NFC:SWNT nanopaper, by filtering the dispersion. (b) Photographs of conductive nanopapers (10 wt % SWNT) showing flexibility and transparency. (c) AFM phase images of a nanopaper surface displaying the random network of interwoven SWNTs and NFC nanofibers. Scalebar 250 nm. (d) (Black) UV−vis absorbance for as prepared SWNT dispersed in NFC (31 wt % SWNT in NFC 0.1 g/L in water), and (red) absorbance of NFC (0.1 g/L in water), (Inset) Absorbance at 500 nm for different concentrations of carboxyl-functionalized SWNTs dispersed in water *vs* the actual concentration calculated from the dry weight. (e) Conductivity of different nanopapers with different weight/volume fractions of SWNT (circle), and a line fitted to a statistical power law percolation theory.

TABLE 1. Mechanical and Electrical Properties of Nanopapers at Different of NFC:SWNT Weight Ratios, and of Anisotropic Microfiber Composites Made from Dispersions at the Dispersion Limit (43 wt % SWNT)

composite type and NFC:SWNT content	Young's modulus (GPa)	tensile strength (MPa)	strain to failure (%)	conductivity (S/cm)
Nanopaper 100% NFC	12.5 ± 0.4	299 ± 8	9.6 ± 0.7	0
Nanopaper 3 wt % SWNT	13.3 ± 0.3	307 ± 6	8.9 ± 0.7	0.03
Nanopaper 10 wt % SWNT	11.2 ± 0.6	213 ± 2	7.0 ± 0.8	3.23
Microfiber 43 wt % SWNT	14[a]	220[a]	2.1[a]	207[a]
100 wt % SWNT-COOH film	25.8 ± 0.9	107 ± 6	0.5 ± 0.1	1029

[a] These values are the highest measured values.

Figure 3e shows the conductivity of different weight ratio composite nanopapers, measured using a four-point probe technique. The figure shows the fit of the conductivity *vs* SWNT volume fraction to statistical power law percolation theory[25]

$$\sigma = \sigma_0(\varphi - \varphi_c)^t$$

where σ_0 = 1029 S cm^{-1} is the measured conductivity of pure SWNT "buckypaper" made from carboxylic acid functionalized SWNTs dispersed in water, φ is the volume fraction of SWNT (calculated from weight using a density of 1.35 g cm^{-3}), φ_c is the percolation threshold, σ is the conductivity of the composite, and the value of t is defined as 2, corresponding to a three-dimensional (3D) random-network percolation system. The percolation threshold φ_c was calculated to 2.7% and the highest measured conductivity was 174 S cm^{-1} at the dispersion limit of this system (43 wt % SWNT). This is the highest reported conductivity for cellulose nanopapers and it is also in the higher conductivity range compared to most other carbon nanotube/polymer composites.[7,26,27] Moreover, these

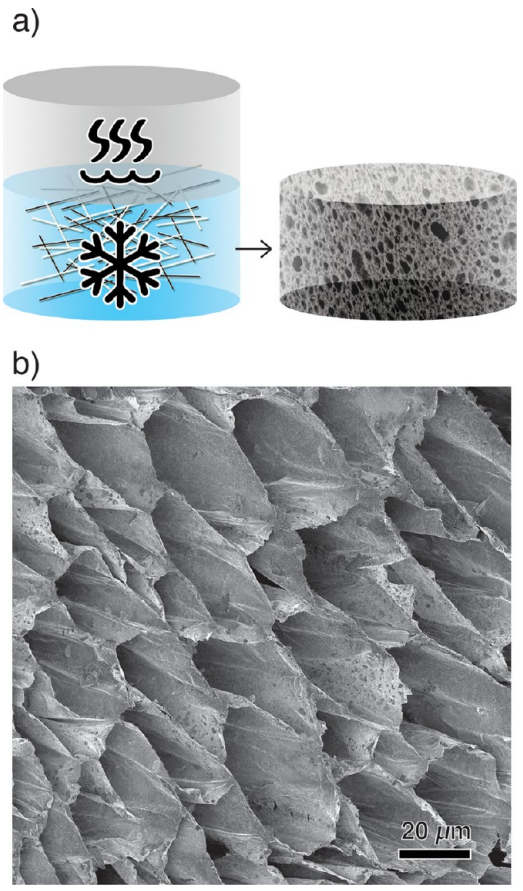

Figure 4. (a) Schematics of the preparation of NFC:SWNT aerogels by first freezing the dispersion followed by freeze-drying. (b) SEM micrograph from the intersection of an NFC:SWNT aerogel (12 wt % SWNT).

conductivities were achieved without significantly degrading the mechanical properties of the already strong pristine nanopaper.

Besides nanopapers, another important emerging class of NFC composites are aerogels.[28,29] The combined NFC aerogel properties of high specific surface area, high mechanical strength and light weight are interesting for many applications, especially when multiple functions are added to the aerogel. Here the addition of SWNTs[15,30] to NFC aerogels have recently been explored using functionalized carbon nanotubes[15] and layer-by-layer assembly of functionalized SWNTs.[30] We managed to successfully manufacture aerogels with the NFC:SWNT dispersions (see Experimental Section and schematics in Figure 4a). The morphology of the aerogels was studied by imaging their cross sections with FE-SEM (Figure 4b). Here a honeycomb structure was observed, which is very similar to that of pure NFC-based aerogels. This indicates that the mechanism for the formation of the honeycomb structure from the NFC:SWNT mixture of nanofibers is similar to that of pure NFC. The formation is a consequence of the directional growth of multiple ice-crystals, where nanofibers are pushed into interstitial regions during freezing. The conductivity of the aerogel in Figure 4b was determined with a 2-point-probe method to be 1.4×10^{-4} S cm^{-1} (12 wt % SWNT). This conductivity value is about 4 orders of magnitude lower than that of the nanopaper. This is reasonable since more than 98 vol % of the aerogel consists of air. The conducting aerogels could be explored in applications such as high surface area biosensors, or in energy storage devices.

As a final and important demonstration, we showed the possibility of aqueous self-assembly of anisotropic nanocomposites from the NFC:SWNT dispersion. This was done by preparation of liquid-extruded microfibers, using a microfluidic-assisted alignment procedure to align the nanoparticles. The general self-assembly process was that the dispersed nanoparticles were first aligned in an accelerated flow inside microfluidic channels. Then the nanoparticles were fixed by inducing a transition from dispersion to gel[31] in the channel, followed by extrusion of the fixed gel fibers (see Experimental Section, and Figure 5a).

The alignment of the NFC and SWNT along the microfiber axis was investigated with Wide Angle X-ray Scattering (WAXS). The radial and azimuthal integrations at (q = 15.8 nm^{-1}) of a diffractogram are seen in Figure 5d,e. Radial integrations of a microfiber with only NFC and of a microfiber containing NFC and SWNT both show the characteristic peak of the cellulose I (200) reflection[32] at q = 15.8 nm^{-1}. The weak peak at q = 18 nm^{-1} apparent in the NFC:SWNT data is not present in the pure NFC WAXS data, and we conclude that this peak originated from the aggregated SWNTs, corresponding to the (002) reflection in the graphite layer.[33] The difference in slope between the curves for the pure NFC and the NFC:SWNT fibers in Figure 5d for q < 12 nm^{-1} can also be explained by graphite packing, where a second peak appears for q < 11 nm^{-1}.

From the azimuthal integration of the cellulose (200) peak at q = 15.8 nm^{-1}, the Herman's order parameter is calculated to be 0.51 in the direction of the fiber (see Experimental Section). This shows that the NFC part of the bicomponent dispersion was indeed aligned in the final composite. We could not, however, find signs of any considerable alignment of the SWNTs along the fiber axis from the WAXS data, due to the weak diffraction signal from the SWNT. SEM images in Figure 5b,c show signs of SWNT striations parallel to the microfiber. Similar results have been reported for monodispersed CNT fiber extrusions.[34] Microfiber cross-sectional SEM pictures also show that nanotubes are oriented to a low degree. These are interesting results as they show that the presence of the SWNT does not disrupt the flow behavior of the NFC even though the SWNT should somehow be coupled to its dispersing agent (the NFC).

For the microfibers with 43 wt % SWNT (the dispersion limit), the highest measured conductivity value

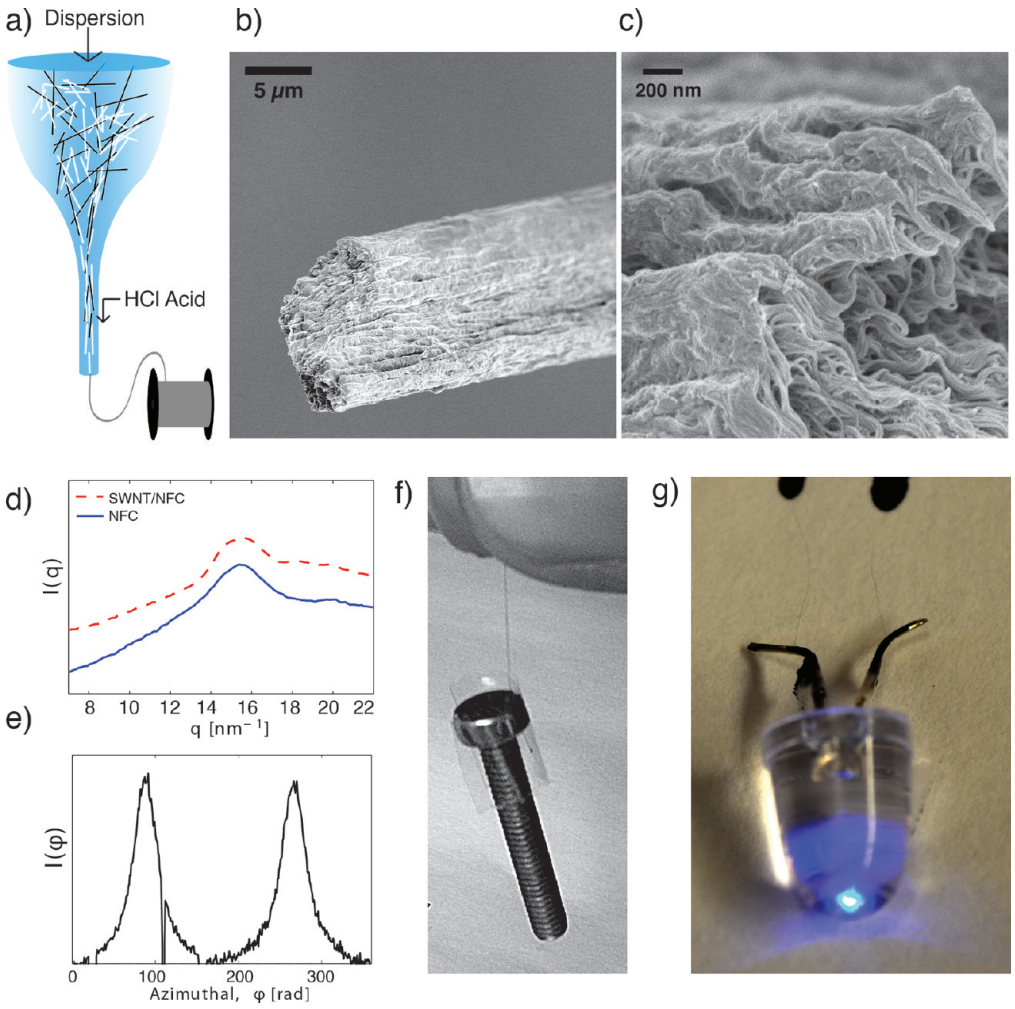

Figure 5. (a) Schematics of the preparation of NFC:SWNT microfibers by injecting the dispersion at the top into a flow-focusing microfluidic system, where the nanofibers are aligned in the focusing sections and the dispersion is gelled by microfluidic injection of an acid (HCl). (b and c) SEM graphs of a microfiber with around 40 wt % SWNT. The fiber intersection is made by cracking the microfiber from the frozen state. (d) The radial integration intensity calculated from Wide Angle X-ray Scattering WAXS data for the NFC:SWNT microfibers displayed in (b) and (c). (e) Azimuthal integration at (q = 15.8 nm^{-1}) from the same WAXS data as in (d). (f) Photograph showing a metal screw suspended using a single NFC:SWNT microfiber. (g) Photograph showing a light emitting diode (20 mW) operating using two single NFC:SWNT (40 wt % SWNT, 10 μm diameter) microfibers as cables.

was 207 S cm^{-1}, which is higher than that of the random-network nanopaper (174 S cm^{-1}). The highest tensile strength for the 43 wt % SWNT microfiber was 220 MPa, with a Young's modulus of 14 GPa. This value of Young's modulus is also higher than that of the random network, which should be an indication of alignment of the NFC fibers.

It should be noted (see Table 1) that the microfiber has a higher Young's modulus than the NFC nanopaper, and a considerably higher tensile strength and strain-to-failure than the SWNT buckypaper.

To demonstrate the combined strength and high conductivity of the 43 wt % ratio NFC:SWNT microfibers, we connected two microfibers (each having around 10 μm diameter and 1 cm in length) to a 20 mW light emitting diode LED, and the LED could be operated at a current density as high as 1400 A cm^{-2} under ambient conditions without breakdown of the microfiber (see Figure 5g). Figure 5f further shows that a 2.6 g object can easily be suspended on the same single microfiber. These results indicate that the NFC:SWNT microfibers could serve as a more sustainable and much more economical alternative to state-of-the-art all-CNT microfibers.[35]

CONCLUSION

We have demonstrated that nanofibrillated cellulose is capable of dispersing and cleaning pristine single-wall carbon nanotubes, resulting in a bicomponent (NFC:SWNT) aqueous dispersion. Our analysis of these dispersions shows high colloidal stability for both components, and high quality in terms of the purity and size of the dispersed SWNT particles. The NFC:SWNT dispersion provides a simple and inexpensive route for self-assembly of advanced hybrid nanocomposites. To show this, we have demonstrated nanopapers, aerogels and

aligned microfiber composites with high strength (stress at break of 200 MPa and a modulus of 14 GPa), and high electrical conductivities above 200 S cm^{-1}).

In future work, dispersions of other types of nanomaterials using NFC could be explored, such as double-wall-, few-wall-, or multiwall nanotubes, graphene, or inorganic nanorods and nanoparticles. Our demonstration of the dispersion of one nanorod using another nanorod is novel, although its mechanisms are not fully understood and should be further explored.

Finally, this study links NFC, which is an emerging, natural, sustainable and inexpensive organic nanomaterial to carbon nanotubes, which is one of the most important synthetic functional nanomaterials. The demonstrated stable dispersions and the high performance of nanocomposites based on these dispersions could be exploited in numerous applications such as microfibers for electronic textiles,[36] nanopaper substrates, inks for low cost printed electronics,[37,38] large-area transparent electrodes,[39] organic bioelectronics,[40,41] functional aerogels,[30] energy storage,[42] and layer-by-layer assembly.[43]

EXPERIMENTAL SECTION

Aqueous Dispersion of NFC:SWNT. The NFC was produced by treating softwood sulfite dissolving pulp with 2 wt % of monochloroacetic acid in order to introduce charged carboxylic groups (550 μequiv g^{-1}) followed by mechanical disintegration with a homogenizer (made and provided by Innventia AB Sweden). The NFC was further purified by diluting 1 g L^{-1} of NFC with shear mixing using IKA T25 Ultra-Turrax at 14000 rpm for 15 min, followed by sonication at 750 W and 50% amplitude in an ice bath with the probe tip diameter of 12 mm for 20 min, and centrifugation at 4500*g* using Beckman Coulter J2 for 1 h where finally 80% of the resulting supernatant was taken. A total of 55 mg of HiPco-produced untreated SWNT from Carbon Solutions, Inc. was added to aqueous NFC dispersion, followed by sonication at 750 W and 50% amplitude in ice bath with a probe tip diameter of 12 mm for 20 min, and centrifugation at 20 000*g* using Beckman Coulter J2 for 1.5 h and 80% of the resulting supernatant was taken. NFC:SWNT dispersion with lower volume fractions of SWNT was prepared by adding NFC from the NFC dispersion to this batch, followed by shear mixing using IKA T25 Ultra-Turrax at 10000 rpm for 5 min.

UV−vis-NIR and the Determination of NFC:SWNT Weight Ratio. Beer−Lambert's law $A = ebc$ (where A is the optical density, e is the extinction coefficient, b is the path length, and c is the concentration) was used to determine the concentration of the final SWNT in the NFC dispersion.[44] The extinction coefficient was determined using carboxyl functionalized SWNTs from the same company (Carbon Solutions, Inc.). The carboxyl functionalized SWNTs were dispersed in water without any other material. The actual concentrations of the different carboxyl-functionalized SWNTs dispersions were determined by measuring the dry content weight of the dispersions. The measured concentrations based on dry-weight were plotted against the UV−vis absorption at 500 nm and a linear calibration was obtained in agreement with the Beer−Lambert's law to find e (see inset in Figure 3d). The calibrated e value was then used to determine the concentration of NFC:SWNT dispersions using absorption at 500 nm. Note that we here assumed that the nonfunctionalized SWNTs have roughly the same absorption per weight as the functionalized SWNTs. All the UV−vis-NIR measurements were done with water as the background reference.

TEM. A dilute sample (0.01 g/L) was deposited on a carbon-coated copper grid (Ultrathin Carbon Film/Holey Carbon, Ted Pella). The excess suspension was removed by blotting with a filter paper. Afterward, the sample was stained with a droplet of fresh solution of uranyl acetate (2 wt % in deionized water), which was added to the grid. The excess solution was removed by blotting with a filter paper and the sample was allowed to dry. A transmission electron microscope (TEM, Hitachi HT-7700, Japan) operated at 80 kV was used to visualize the dispersion.

SEM. Scanning electron microscopy (SEM) images were captured using the high-vacuum instrument Hitachi S-4800 (Hitachi Corp., Japan) equipped with a field emission electron gun. The following settings were used: 0.7−1 kV in acceleration voltage, a probe current of 5−10 μA, and a working distance of 4−8 mm and using a secondary electron detector. All samples were sputtered for 15 s with platinum−palladium. To image the cross section, the aerogels were cut with a sharp razor blade. The microfibers were submerged in liquid nitrogen and cracked in the liquid to create cross sections for imaging.

AFM. Images were captured with a multiomode Nanoscope IIIa Atomic Force Microscope (AFM) produced by Bruker Corp. The AFM was operated in the tapping mode, and RTESP7 cantilevers, having a nominal tip radius of 8 nm and a spring constant of 40 N/m (Bruker Corp.), were used. Images were captured both from surface of the free-standing films (described above) and from silica wafers onto which a small volume of a 0.01 g/L NFC:SWNT dispersion had been cast.

DLS. The Zetasizer ZEN3600 instrument from Malvern Instruments Ltd., U.K. was used for the dynamic light scattering (DLS) measurements. One milliliter of sample was placed in disposable polystyrene cuvettes. The measurements were performed at 25 °C and each of the curves is the average of 10 s measurements.

Preparation and Characterization of Nanopapers. NFC:SWNT dispersions with a given ratio were vacuum-filtered using hydrophobic polyvinyl difluoride (PVDF) Millipore membrane filters with 0.65 μm poresize (Durapore), followed by sheet forming using Rapid Köthen, RK3A-KWT PTI at a vacuum pressure of −1 bar at 90 °C for 15 min. Mechanical properties of the papers were evaluated using tensile test under controlled conditions of 50% RH, 23 °C. Specimens of 50 mm length, 5 mm width and thickness of 10 μm were tested using Universal Material Testing Machine Instron 5944 equipped with 500 N load cell with cross-head speed of 5 mm/min corresponding to an initial strain rate of 10%/min. Data from 5 different specimens was collected to obtain a statistical error for each sample type .

UV−vis-NIR spectra of the dispersions were collected using a UV-2550 Shimadzu spectrophotometer. Raman spectroscopy of NFC:SWNT dispersion was performed using Perkin-Elmer Spectrum 2000 in 100 mW with 64 individual scans at a resolution of 2 cm^{-1}. The electrical conductivity of the papers was measured with a four-point probe Van der Pauw setup using Solartron SI1287 with graphite electrodes on the circumference of the paper.

Preparation and Analysis of Aerogels. Starting NFC:SWNT dispersions (1 g/L, 12 wt % SWNT) were concentrated by slow heating to semidilute state at a concentration of about 3 g/L. The semidilute dispersion was then gelled in an aluminum cup (30 mm in diameter) by adding a few drops of sodium chloride solution (1 M). The gel was subsequently cooled with liquid nitrogen, followed by freeze-drying. The conductivity was measured using a 2-point probe measurement by painting two silver electrodes on each side of the aerogel. Here we assumed that the contact resistance is negligible compared to the resistance measured through the aerogel. The width, height and depth of the aerogel were determined by using a micrometer caliper.

Preparation and Analysis of Microfibers. A 3 g/L dispersion consisting of 10 wt % SWNT and 90 wt % NFC was used to prepare the microfibers. The flow-focusing setup consisted of six microfluidic channels, with five inlets and one outlet. All six channels in the flow-focusing setup have a square cross section with a side of 1 mm. The inlets are 45 mm long and the outlet 47 mm. The channels were cut from a 1 mm thick stainless steel plate, which in turn was sandwiched between two PMMA plates (see Figure 3S for photos and schematics). Three syringe pumps (Aladdin NE-4000, WPI) fed the channels, with the NFC:SWNT dispersion injected at a volume flow rate $Q_1 = 3.9$ mL/h. The first side flow at $Q_2 = 9.4$ mL/h consisted of deionized water (Milli-Q) while the second at $Q_3 = 47$ mL/h was dilute HCl with pH = 2. The gel fiber, formed in the setup, was ejected from the submerged outlet into an HCl bath at pH = 2 Thereafter, the gel fiber was transferred from the pH = 2 bath and stored in a deionized water bath for 24 h. The fiber was then taken out and hung to dry in air with fixed end points.

The conductivity was measured using a 2-point probe measurement by painting two silver electrodes around the fiber. The distance between the electrodes was measured with an optical microscope, and the diameter of the fiber was measured by averaging 10 different diameters measured between the electrodes, using optical microscope. Here we assumed that the electrode resistance was negligible as compared to the absolute resistance of the fiber between the electrodes, which varied in the range of 25 000−80 000 Ω depending on the differences in fibers geometries and electrode distances. The LED experiment was done by using silver and carbon paint for connecting individual fibers to each leg of the LED. A Keithly 2400 was used to drive the LED.

Wide Angle X-ray Scattering Microfibers. WAXS measurements were carried out at the P03 beamline at the electron storage ring PETRA III at DESY in Hamburg, Germany. The transmission experiments were performed with an X-ray beam with the wavelength of 0.957 Å and the beam area of 26 × 17 μm^2. The sample to detector distance was 95 mm and the setup was calibrated with Al_2O_3. The scattering patterns were recorded using a Pilatus300K detector (Dectris) with a pixel size of 172 × 172 μm^2 (see Figure 4S), The alignment and Herman's order parameter H, was calculated using the equation

$$H = \left\langle \frac{3}{2}\cos^2\phi - \frac{1}{2} \right\rangle$$

where φ is the azimuthal angle.

Conflict of Interest: The authors declare no competing financial interest.

Acknowledgment. We thank Koshi H for graphics production, and Erdem Karabulut for discussions on the dispersion mechanism. We acknowledge funding from the Wallenberg Wood Science Centre, and from the Power paper project at Linköping University, both funded by the Knut and Alice Wallenberg (KAW) Research Foundation.

Supporting Information Available: Stress−strain data for nanopapers, TEM magnified image of NFC:SWNT bundle, WAXS data, photos and schematics of microfiber extruder. This material is available free of charge *via* the Internet at http://pubs.acs.org.

REFERENCES AND NOTES

1. De Volder, M. F. L.; Tawfick, S. H.; Baughman, R. H.; Hart, A. J. Carbon Nanotubes: Present and Future Commercial Applications. *Science* **2013**, *339*, 535–539.
2. Wong, E. W. Nanobeam Mechanics: Elasticity, Strength, and Toughness of Nanorods and Nanotubes. *Science* **1997**, *277*, 1971–1975.
3. Treacy, M. M. J.; Ebbesen, T. W.; Gibson, J. M. Excpetionally High Young's Modulus Observed for Individual Carbon Nanotubes. *Nature* **1996**, *381*, 678–680.
4. Hou, Y.; Tang, J.; Zhang, H.; Qian, C.; Feng, Y.; Liu, J. Functionalized Few-Walled Carbon Nanotubes for Mechanical Reinforcement of Polymeric Composites. *ACS Nano* **2009**, *3*, 1057–1062.
5. Premkumar, T.; Mezzenga, R.; Geckeler, K. E. Carbon Nanotubes in the Liquid Phase: Addressing the Issue of Dispersion. *Small* **2012**, *8*, 1299–1313.
6. Dzenis, Y. Materials Science. Structural Nanocomposites. *Science* **2008**, *319*, 419–420.
7. Sahoo, N. G.; Rana, S.; Cho, J. W.; Li, L.; Chan, S. H. Polymer Nanocomposites Based on Functionalized Carbon Nanotubes. *Prog. Polym. Sci.* **2010**, *35*, 837–867.
8. Li, E. Y.; Marzari, N. Improving the Electrical Conductivity of Carbon Nanotube Networks: A First-Principles Study. *ACS Nano* **2011**, *5*, 9726–9736.
9. Moon, R. J.; Martini, A.; Nairn, J.; Simonsen, J.; Youngblood, J. Cellulose Nanomaterials Review: Structure, Properties and Nanocomposites. *Chem. Soc. Rev.* **2011**, *40*, 3941–3994.
10. Klemm, D.; Kramer, F.; Moritz, S.; Lindström, T.; Ankerfors, M.; Gray, D.; Dorris, A. Nanocelluloses: A New Family of Nature-Based Materials. *Angew. Chem., Int. Ed.* **2011**, *50*, 5438–5466.
11. Iwamoto, S.; Kai, W.; Isogai, A.; Iwata, T. Elastic Modulus of Single Cellulose Microfibrils from Tunicate Measured by Atomic Force Microscopy. *Biomacromolecules* **2009**, *10*, 2571–2576.
12. Fukuzumi, H.; Saito, T.; Iwata, T.; Kumamoto, Y.; Isogai, A. Transparent and High Gas Barrier Films of Cellulose Nanofibers Prepared by TEMPO-Mediated Oxidation. *Biomacromolecules* **2009**, *10*, 162–165.
13. Berglund, L. A.; Peijs, T. Cellulose Biocomposites—From Bulk Moldings to Nanostructured Systems. *MRS Bull.* **2010**, *35*, 201–208.
14. Salajkova, M.; Valentini, L.; Zhou, Q.; Berglund, L. Tough and Conductive Nanopaper Structures Based on Cellulose Nanofibrils and Carbon Nanotubes. *Compos. Sci. Technol.* **2013**, *87*, 103–110.
15. Wang, M.; Anoshkin, I. V.; Nasibulin, A. G.; Korhonen, J. T.; Seitsonen, J.; Pere, J.; Kauppinen, E. I.; Ras, R. H. A.; Ikkala, O. Modifying Native Nanocellulose Aerogels with Carbon Nanotubes for Mechanoresponsive Conductivity and Pressure Sensing. *Adv. Mater.* **2013**, *25*, 2428–2432.
16. Koga, H.; Saito, T.; Kitaoka, T.; Nogi, M.; Suganuma, K.; Isogai, A. Transparent, Conductive, and Printable Composites Consisting of TEMPO-Oxidized Nanocellulose and Carbon Nanotube. *Biomacromolecules* **2013**, *14*, 1160–1165.
17. Wågberg, L.; Decher, G.; Norgren, M.; Lindström, T.; Ankerfors, M.; Axnäs, K. The Build-Up of Polyelectrolyte Multilayers of Microfibrillated Cellulose and Cationic Polyelectrolytes. *Langmuir* **2008**, *24*, 784–795.
18. Yu, A.; Bekyarova, E.; Itkis, M. E.; Fakhrutdinov, D.; Webster, R.; Haddon, R. C. Application of Centrifugation to the Large-Scale Purification of Electric Arc-Produced Single-Walled Carbon Nanotubes. *J. Am. Chem. Soc.* **2006**, *128*, 9902–9908.
19. Kataura, H.; Kumazawa, Y.; Maniwa, Y.; Ohtsuka, Y.; Sen, R.; Suzuki, S.; Achiba, Y. Diameter Control of Single-Walled Carbon Nanotubes. *Carbon* **2000**, *38*, 1691–1697.
20. Takahashi, T.; Tsunoda, K.; Yajima, H.; Ishii, T. Dispersion and Purification of Single-Wall Carbon Nanotubes Using Carboxymethylcellulose. *Jpn. J. Appl. Phys.* **2004**, *43*, 3636–3639.
21. Shinoda, R.; Saito, T.; Okita, Y.; Isogai, A. Relationship Between Length and Degree of Polymerization of TEMPO-Oxidized Cellulose Nanofibrils. *Biomacromolecules* **2012**, *13*, 842–849.
22. Minami, N.; Kim, Y.; Miyashita, K.; Kazaoui, S.; Nalini, B. Cellulose Derivatives as Excellent Dispersants for Single-Wall Carbon Nanotubes as Demonstrated by Absorption and Photoluminescence Spectroscopy. *Appl. Phys. Lett.* **2006**, *88*, 093123−093123–3.
23. Olivier, C.; Moreau, C.; Bertoncini, P.; Bizot, H.; Chauvet, O.; Cathala, B. Cellulose Nanocrystal-Assisted Dispersion of Luminescent Single-Walled Carbon Nanotubes for

Layer-by-Layer Assembled Hybrid Thin Films. *Langmuir* **2012**, *28*, 12463–12471.
24. Gustafsson, E.; Johansson, E.; Wågberg, L.; Pettersson, T. Direct Adhesive Measurements between Wood Biopolymer Model Surfaces. *Biomacromolecules* **2012**, *13*, 3046–3053.
25. Hu, L.; Hecht, D. S.; Grüner, G. Percolation in Transparent and Conducting Carbon Nanotube Networks. *Nano Lett.* **2004**, *4*, 2513–2517.
26. Chen, T.; Cai, Z.; Qiu, L.; Li, H.; Ren, J.; Lin, H.; Yang, Z.; Sun, X.; Peng, H. Synthesis of Aligned Carbon Nanotube Composite Fibers with High Performances by Electrochemical Deposition. *J. Mater. Chem. A* **2013**, *1*, 2211–2216.
27. Guo, W.; Liu, C.; Sun, X.; Yang, Z.; Kia, H. G.; Peng, H. Aligned Carbon Nanotube/Polymer Composite Fibers with Improved Mechanical Strength and Electrical Conductivity. *J. Mater. Chem.* **2012**, *22*, 903–908.
28. Pääkkö, M.; Vapaavuori, J.; Silvennoinen, R.; Kosonen, H.; Ankerfors, M.; Lindström, T.; Berglund, L. a.; Ikkala, O. Long and Entangled Native Cellulose I Nanofibers Allow Flexible Aerogels and Hierarchically Porous Templates for Functionalities. *Soft Matter* **2008**, *4*, 2492–2499.
29. Olsson, R. T.; Azizi Samir, M. a S.; Salazar-Alvarez, G.; Belova, L.; Ström, V.; Berglund, L. a; Ikkala, O.; Nogués, J.; Gedde, U. W. Making Flexible Magnetic Aerogels and Stiff Magnetic Nanopaper Using Cellulose Nanofibrils as Templates. *Nat. Nanotechnol.* **2010**, *5*, 584–588.
30. Hamedi, M.; Karabulut, E.; Marais, A.; Herland, A.; Nyström, G.; Wågberg, L. Nanocellulose Aerogels Functionalized by Rapid Layer-by-Layer Assembly for High Charge Storage and Beyond. *Angew. Chem., Int. Ed.* **2013**, *52*, 12038–12042.
31. Fall, A. B.; Lindström, S. B.; Sundman, O.; Ödberg, L.; Wågberg, L. Colloidal Stability of Aqueous Nanofibrillated Cellulose Dispersions. *Langmuir* **2011**, *27*, 11332–11338.
32. Sugiyama, J.; Vuong, R.; Chanzy, H. Electron Diffraction Study on the Two Crystalline Phases Occurring in Native Cellulose from an Algal Cell Wall. *Macromolecules* **1991**, *24*, 4168–4175.
33. Nogales, A.; Hernández, J. J.; Rueda, D. R.; Ezquerra, T. A. X-Ray Scattering Applied to the Analysis of Carbon Nanotubes, Polymers and Nanocomposites. *Opt. Pura Apl.* **2007**, *2279*, 195–205.
34. Baughman, R. H. Putting a New Spin on Carbon Nanotubes. *Science* **2000**, *290*, 1310–1311.
35. Behabtu, N.; Young, C. C.; Tsentalovich, D. E.; Kleinerman, O.; Wang, X.; Ma, A. W. K.; Bengio, E. A.; ter Waarbeek, R. F.; de Jong, J. J.; Hoogerwerf, R. E.; *et al.* Strong, Light, Multifunctional Fibers of Carbon Nanotubes with Ultrahigh Conductivity. *Science* **2013**, *339*, 182–186.
36. Hamedi, M.; Forchheimer, R.; Inganäs, O. Towards Woven Logic from Organic Electronic Fibres. *Nat. Mater.* **2007**, *6*, 357–362.
37. Forrest, S. R. The Path to Ubiquitous and Low-Cost Organic Electronic Appliances on Plastic. *Nature* **2004**, *428*, 911–918.
38. Huang, J.; Zhu, H.; Chen, Y.; Preston, C.; Rohrbach, K.; Cumings, J.; Hu, L. Highly Transparent and Flexible Nanopaper Transistors. *ACS Nano* **2013**, *7*, 2106–2113.
39. Hu, L.; Zheng, G.; Yao, J.; Liu, N.; Weil, B.; Eskilsson, M.; Karabulut, E.; Ruan, Z.; Fan, S.; Bloking, J. T.; *et al.* Transparent and Conductive Paper from Nanocellulose Fibers. *Energy Environ. Sci.* **2013**, *6*, 513–518.
40. Berggren, M.; Richter-Dahlfors, A. Organic Bioelectronics. *Adv. Mater.* **2007**, *19*, 3201–3213.
41. Shin, S. R.; Jung, S. M.; Zalabany, M.; Kim, K.; Zorlutuna, P.; Kim, S.; Nikkhah, M.; Khabiry, M.; Azize, M.; Kong, J.; *et al.* Carbon-Nanotube-Embedded Hydrogel Sheets for Engineering Cardiac Constructs and Bioactuators. *ACS Nano* **2013**, 2369–2380.
42. Gui, Z.; Zhu, H.; Gillette, E.; Han, X.; Rubloff, G. W.; Hu, L.; Lee, S. B. Natural Cellulose Fiber as Substrate for Supercapacitor. *ACS Nano* **2013**, *7*, 6037–6046.
43. Lee, S. W.; Kim, B.; Chen, S.; Shao-horn, Y.; Hammond, P. T. Layer-by-Layer Assembly of All Carbon Nanotube Ultrathin Films for Electrochemical Applications. *J. Am. Chem. Soc.* **2009**, *131*, 671–679.
44. Bahr, J. L.; Mickelson, E. T.; Bronikowski, M. J.; Smalley, R. E.; Tour, J. M. Dissolution of Small Diameter Single-Wall Carbon Nanotubes in Organic Solvents?. *Chem. Commun.* **2001**, 193–194.